Provided for non-commercial research and education use.
Not for reproduction, distribution or commercial use.

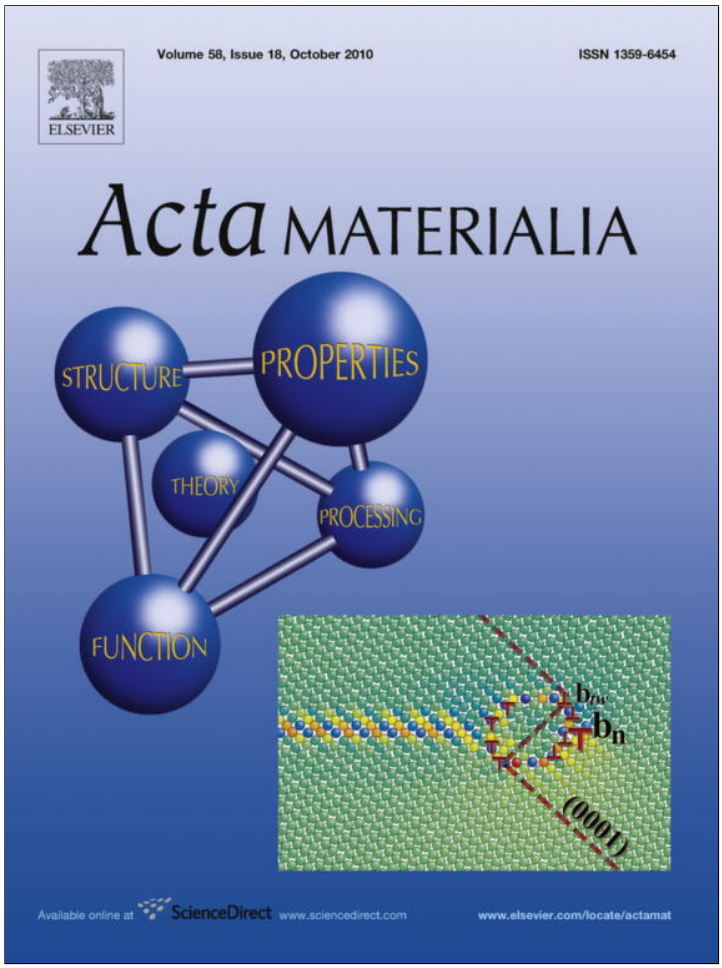

This article appeared in a journal published by Elsevier. The attached copy is furnished to the author for internal non-commercial research and education use, including for instruction at the authors institution and sharing with colleagues.

Other uses, including reproduction and distribution, or selling or licensing copies, or posting to personal, institutional or third party websites are prohibited.

In most cases authors are permitted to post their version of the article (e.g. in Word or Tex form) to their personal website or institutional repository. Authors requiring further information regarding Elsevier's archiving and manuscript policies are encouraged to visit:

http://www.elsevier.com/copyright

Author's personal copy

Available online at www.sciencedirect.com
ScienceDirect
Acta Materialia 58 (2010) 6206–6215
Acta MATERIALIA
www.elsevier.com/locate/actamat

Strain glass in Fe-doped Ti–Ni

Dong Wang [a,b,d], Zhen Zhang [a,b], Jian Zhang [a,b], Yumei Zhou [a,b], Yu Wang [a,c], Xiangdong Ding [a,b], Yunzhi Wang [a,d], Xiaobing Ren [a,b,c,*]

[a] Multi-disciplinary Materials Research Center, Frontier Institute of Science and Technology, Xi'an Jiaotong University, Xi'an 710049, China
[b] State Key Laboratory for Mechanical Behavior of Materials, Xi'an Jiaotong University, Xi'an 710049, China
[c] Ferroic Physics Group, National Institute for Materials Science, Tsukuba, 305-0047 Ibaraki, Japan
[d] Department of Materials Science and Engineering, The Ohio State University, 2041 College Road, Columbus, OH 43210, USA

Received 22 January 2010; received in revised form 3 July 2010; accepted 26 July 2010
Available online 20 August 2010

Abstract

We report the existence of strain glass in $Ti_{50}Ni_{50-x}Fe_x$, beyond a critical Fe doping level $x > x_c (5 < x_c < 6)$. The strain glass state is confirmed by the appearance of a frequency-dependent anomaly in the AC mechanical modulus/loss at a freezing temperature T_0 and by the breaking of ergodicity shown in a zero-field-cooling/field-cooling experiment. Based on the experimental results, a phase diagram is established in which both the normal martensitic transformations (for $x < x_c$) and the strain glass transition (for $x > x_c$) are indicated. The new phase diagram allows for explanations of two long-standing puzzles in $Ti_{50}Ni_{50-x}Fe_x$ and Ti–Ni alloys: (i) the origin of nano-domains present prior to the martensitic transformation (for $x < x_c$) and (ii) the negative temperature dependence of electrical resistivity in abnormal non-transforming compositions (for $x > x_c$).
© 2010 Acta Materialia Inc. Published by Elsevier Ltd. All rights reserved.

Keywords: Ferroelastic; Martensitic phase transformation; Strain glass; Nano-domains; Dynamic mechanical analyzer (DMA)

1. Introduction

Strain glass is a new form of glass state found very recently in ferroelastic Ti–Ni systems [1,2]. It is a frozen state of local lattice strains. Unlike a normal martensitic crystal (long-range strain ordered state, i.e. strain-crystal state), a strain glass on the one hand exhibits no breaking of the parent phase symmetry at all temperatures (as observed by X-ray diffractometry), behaving like a common non-transforming system, but on the other hand exhibits important glass transition features such as dynamic freezing measured by dynamic modulus analysis (DMA) experiments [1], and breaking down of ergodicity measured by zero-field-cooling/field-cooling (ZFC/FC) experiments [2], which are signatures of a typical freezing process, are parallel to those found in spin glasses [3,4] of ferromagnetic systems and relaxors [5–7] of ferroelectric systems. Strain glass in Ti–Ni has been found to exhibit a number of interesting novel properties, including shape memory effect and superelasticity [8,9]. This indicates that strain glass may have a potential for promising applications.

Strain glass in Ti–Ni shows a number of features similar to the "precursory phenomena" prior to a martensitic transformation, such as the appearance of nano-domains, modulus softening, abnormal negative temperature dependent of electrical resistivity and the appearance of diffuse scatterings near 1/3 $\langle 1\,1\,0 \rangle$ [10–15]. Long before the experimental discovery of strain glass, several early theoretical models [12,16,17] have made an important prediction that a "spin-glass-like" state may exist in martensitic systems, but they considered the pre-martensitic tweed as corresponding to such a state. Nevertheless, recent experiment [18] has shown that the pre-martensitic state is yet to be a glass phase, and there is a clear difference between strain glass and pre-martensitic tweed. A strain

* Corresponding author at: Ferroic Physics Group, National Institute for Materials Science, Tsukuba, 305-0047, Ibaraki, Japan. Tel.: +81 298 59 2731; fax: +81 298 59 2701.
E-mail address: Ren.Xiaobing@nims.go.jp (X. Ren).

1359-6454/$36.00 © 2010 Acta Materialia Inc. Published by Elsevier Ltd. All rights reserved.
doi:10.1016/j.actamat.2010.07.040

Author's personal copy

glass transition undergoes a freezing process, which manifests itself by the appearance of a frequency-dependent internal friction peak in the AC mechanical susceptibility measurement (i.e. DMA) [1] and a zero-field-cooling peak in DC strain measurement [2]. These signatures are caused by the freezing of randomly distributed nano-scale strain domains. By contrast, the precursory state prior to a martensitic transformation does not show these "freezing" characteristics, as evidenced by the absence of the above-mentioned anomalies in AC and DC mechanical measurements [18]. Distinguishing clearly the strain glass state from the pre-martensitic state may help solve two long-standing puzzles associated with the pre-martensitic state and abnormal non-transforming compositions of Ti–Ni and Ti–Ni–Fe systems [13–15,19–22]; one is the origin of nano-domains prior to the normal martensitic transformation and the other is the abnormal "negative temperature dependence" of the electrical resistivity in the abnormal non-transforming alloys.

It has been proposed that strain glass can be achieved by doping sufficient point defects into a ferroelastic system so as to prevent the long-range strain ordering (i.e. martensitic transformation) [23]. The first strain glass was reported in a water-quenched Ni-rich $Ti_{50-x}Ni_{50+x}$ binary system [1], which can be viewed as self-doping of excess Ni into a defect-free $Ti_{50}Ni_{50}$. Doping excess Ni over a critical value ($x > 1$) suppresses the B2–B19′ martensitic transformation [1,24,25] and the system undergoes a freezing transition into a randomly distributed R-like nano-domains (which is nano-sized R strain domains) [2,26]. Therefore, the binary $Ti_{50-x}Ni_{50+x}$ system is characterized by a strain glass (short-range strain order with R-phase structure) whose structure is different from the corresponding martensite (long-range strain order with B19′ structure).

Since strain glass is relatively a new phenomenon, it is of fundamental interest to know if it could be found in other ferroelastic systems and, in particular, if the relation between the local strain order and long-range strain order is always different or could be the same. In this paper, we report a new and simpler strain glass system, $Ti_{50}Ni_{50-x}Fe_x$, where the strain glass state has the same strain order as that of the martensitic phase (i.e. both are R-phase). We found that the addition of Fe suppresses the B2–R martensitic transformation [24] and leads to a strain glass transition with R-like nano-domains. Thus both the long-range and short-range strain orders in $Ti_{50}Ni_{50-x}Fe_x$ have the same R-phase structure. This finding suggests that $Ti_{50}Ni_{50-x}Fe_x$ could serve as a prototypical system for strain glass study.

The systematic study on the transformation behavior of $Ti_{50}Ni_{50-x}Fe_x$ with different Fe content ($2 \leqslant x \leqslant 10$) presented in this paper has allowed for the establishment of a phase diagram of the system incorporating martensite, strain glass, and precursory nano-domains state prior to martensitic or strain glass transformations. The phase diagram demonstrates clearly the relationship among the well-observed precursory nano-domains state, the martensitic state and the strain glass state. It was also found that the long-standing puzzle – "negative temperature dependence" of electrical resistivity in the pre-martensitic state and in the abnormal non-transforming compositions of Ti–Ni and Ti–Ni–Fe systems [13–15,21,22] – can be easily understood by the existence of the static R nano-domains.

2. Experimental

Samples of $Ti_{50}Ni_{50-x}Fe_x$ alloys with $x = 2$, 3, 4, 5, 6, 6.5, 7, 8 and 10 were prepared by induction melting of high purity metals (>99.9%). All the ingots were heat treated at 1273 K for 24 h in evacuated quartz tubes to eliminate compositional non-uniformities. The samples were then cut into suitable shapes for different experiments ($3 \times 3 \times 1$ mm^3 for differential scanning calorimetry (DSC), long bars for electrical resistivity, $2 \times 2 \times 60$ mm^3 for DMA, and $6 \times 6 \times 2$ mm^3 for X-ray diffraction (XRD)). The samples were finally solution-treated at 1273 K for 1 h followed by water-quench. All the samples were etched with $HF:HNO_3:H_2O$ 1:4:5 (in volume) solution to remove oxidized surface layers.

The XRD experiments were done by using Shimadzu XRD7000 with a cooling holder to detect possible structural changes with temperature. The DSC experiments were carried out on TA Q200 with a cooling and heating rate of 10 K min^{-1} between 323 and 123 K. The "four probe method" with a constant current 100 mA was used to measure the electrical resistivity. The dynamical mechanical properties were obtained by TA Q800 DMA using the single cantilever mode with amplitude of 15 μm (AC field frequency from 0.2 to 20 Hz). The temperature was chosen from 323 to 133 K with step cooling mode. The ZFC/FC (zero-field-cooling/field-cooling) experiments were done by using TA Q800 DMA with tensile mode at a small stress ~30 MPa. The experimental details of ZFC/FC measurement can be found in Ref. [2]. The ZFC is not completely stress-free (as a small preset stress is need to keep the sample straight), but this does not affect the detection of non-ergodicity. The diffuse scattering caused by nano-domains was observed by transmission electron microscopy (TEM) using a JEM-2000EX microscope with a liquid nitrogen cooling holder.

3. Results

3.1. Effect of Fe doping on transformation behavior of $Ti_{50}Ni_{50-x}Fe_x$ system: crossover from normal martensitic transformation to "abnormal non-transforming state"

Now we show that Fe doping causes a crossover at a critical doping level ($5 < x_c < 6$) from a normal martensitic transformation (R or B19′) to an abnormal non-transforming behavior.

Fig. 1a–c shows the XRD spectra of $Ti_{50}Ni_{50-x}Fe_x$ alloys with $x = 2$, 4, and 6, respectively. An analysis of the XRD results suggests that $Ti_{50}Ni_{48}Fe_2$ undergoes

Author's personal copy

B2–R–B19′ two-step martensitic transformations (Fig. 1a) while $Ti_{50}Ni_{46}Fe_4$ undergoes a B2–R one-step martensitic transformation without subsequent transforming into B19′ martensite (Fig. 1b). In contrast, the XRD spectra of $Ti_{50}Ni_{44}Fe_6$ show no phase transformation (e.g. the B2 peak remains unchanged) within the temperature range considered (from 298 K down to 93 K). Nevertheless, the B2 peak becomes broader with decreasing temperature, as shown in Fig. 1d. This anomalous peak broadening seems to suggest that some subtle changes exist in this seemingly non-transforming alloy.

Fig. 2 shows the variation of DSC cooling curves with Fe doping level ($x = 2$–10). It can be seen that at low doping level ($x = 2$–5) the martensitic transformation(s) are accompanied by large and sharp exothermic peaks in the DSC curves. With the increase of Fe content, the exothermic peak shifts to the low temperature side, suggesting that the martensitic transformation temperature lowers drastically with increasing doping level. The two peaks for $x = 2$ correspond to B2–R and R–B19′ two-stage martensitic transformation, whereas the single peak for $x = 3$–5 corresponds to the B2–R one-stage martensitic transformation. The most interesting result from Fig. 2, which has also been reported in Refs. [14,15], is that the DSC peak becomes smaller and broader with increasing Fe doping level and for $x \geqslant 6$, the DSC peak virtually vanishes. It is replaced by a very broad and weak hump, which is less sensitive to further Fe doping. Clearly, the broad and weak DSC hump is quite different from that of a normal martensitic transformation. Note that the composition range with no DSC peaks (i.e. $x = 6$–10) coincide with the non-transforming compositions revealed in the XRD analysis above.

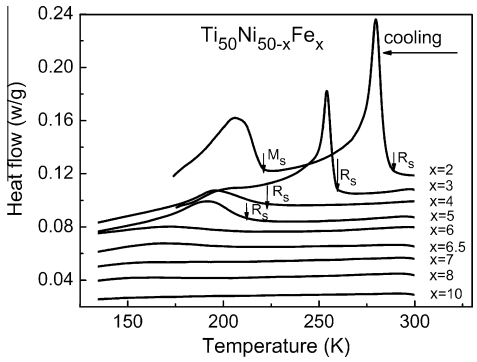

Fig. 2. DSC curves of $Ti_{50}Ni_{50-x}Fe_x$ alloys with different Fe content ($x = 2$–10) upon cooling. R_s and M_s represent R-phase transformation start temperature and B19′ phase transformation start temperature, respectively.

The variation of the electrical resistivity curves with Fe doping level ($x = 2$–10) is shown in Fig. 3. All the results are normalized by the electrical resistivity at 293 K. Similar to what was found in the DSC measurement, increasing Fe doping level results in interesting changes in the transformation behavior. At low Fe doping level $x = 2$–5, there exists a sharp change (with a hysteresis between heating and cooling) in resistivity accompanying the martensitic

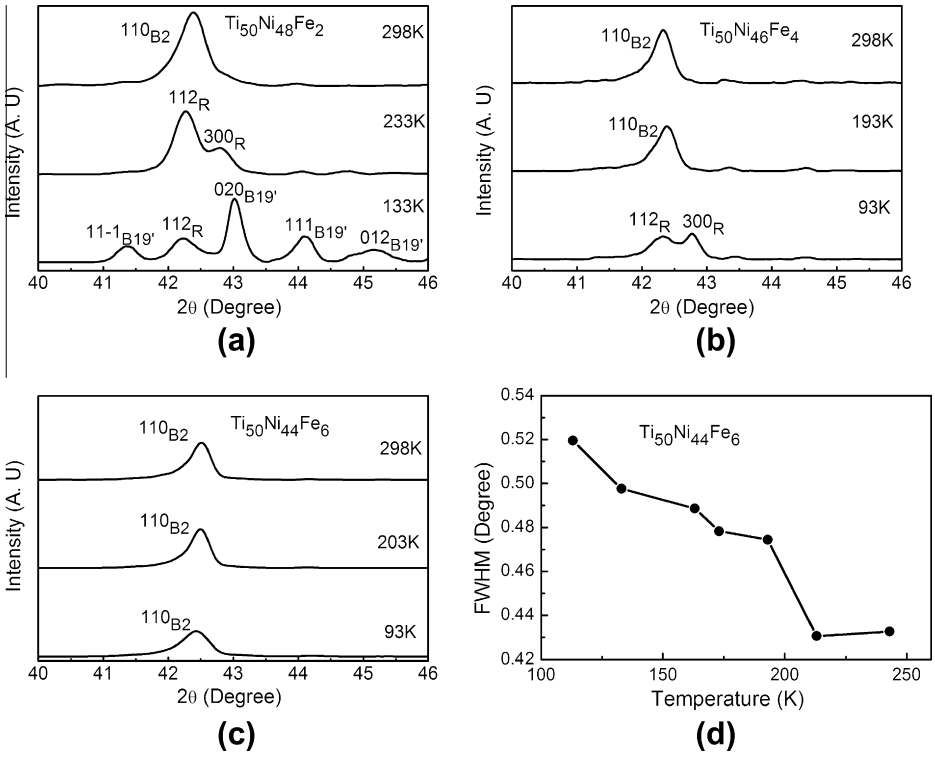

Fig. 1. XRD profiles of $Ti_{50}Ni_{48}Fe_2$ (a) $Ti_{50}Ni_{46}Fe_4$ (b), and $Ti_{50}Ni_{44}Fe_6$ (c) at different temperatures. AU stands for arbitrary units. The temperature dependence of the full width at half maximum (FWHM) of $Ti_{50}Ni_{44}Fe_6$ ($1\ 1\ 0_{B2}$) peaks is shown in (d).

Author's personal copy

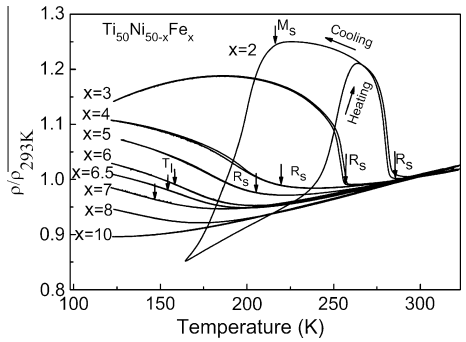

Fig. 3. Normalized (at 293 K) electrical resistivity curves (for both cooling and heating) of $Ti_{50}Ni_{50-x}Fe_x$ at different Fe content ($x = 2$–10). R_s and M_s represent R-phase transformation start temperature and B19′ transformation start temperature, respectively. The arrows in $x = 6$, $x = 6.5$ and $x = 7$ indicate the inflection point (T_I) of the electrical resistivity curves obtained for alloys of "non-transforming" compositions.

transformation B2–R or R–B19′. This is expected for a martensitic transformation. With further increasing Fe doping level, the resistivity change at the martensitic transformation temperatures (R_s and M_s) becomes weaker and weaker. For $x \geqslant 6$, there is no signature for martensitic transformation (first order transformation) any more, as no hysteresis exists in any temperature range. However, there exists an anomalous increase in resistivity below a certain temperature for these heavily doped compositions. Such anomalous increase in resistivity is known as the "negative temperature dependence" of resistivity [13,22]. We note that the anomalous behavior of resistivity in the heavily doped compositions ($x \geqslant 6$) coincides with the anomaly in DSC curves of the same compositions; this is another feature of the abnormal non-transforming compositions.

All the above results converge to one important phenomenon: Fe doping significantly changes the transformation behavior of $Ti_{50}Ni_{50-x}Fe_x$ and there exists a crossover from a normal martensitic transformation (B2–R) to an abnormal non-transforming state when Fe doping exceeds a critical concentration x_c ($5 < x_c < 6$)). The change of transformation behavior with Fe doping has been studied previously [14,15,19,20,27] and the appearance of a strange state (with a negative temperature dependence of resistivity) at high Fe doping level has also been reported [14,15,21,22]. Our results above are in agreement with these previous studies [14,15,22]. However, the nature and the origin of the crossover and the abnormal non-transforming state have remained unclear. In the following we shall show evidence that the non-transforming state actually corresponds to a strain glass state.

3.2. Evidence for strain glass in $Ti_{50}Ni_{50-x}Fe_x$ when $x \geqslant 6$

A dynamic mechanical analyzer (DMA) was employed to detect strain glass transition in $Ti_{50}Ni_{50-x}Fe_x$. Fig. 4 shows the DMA results of $Ti_{50}Ni_{50-x}Fe_x$ alloys having different x values. The DSC curves are also shown in the figures for comparison. Fig. 4a–c shows the DMA results obtained for alloys of low Fe compositions, i.e. $x = 2$, 4, and 5. The B2–R martensitic transformation starting temperature (dashed line) determined by the DSC curves is consistent with the starting temperature of the storage modulus dip and the starting temperature of the internal friction peak. For $x = 2$, the internal friction peak at low temperature (~220 K) corresponds to the R–B19′ transformation. The martensitic transformation of these transforming compositions ($x \leqslant 5$) is characterized by a frequency-independent DMA dip and a large frequency-independent internal friction peak (i.e. no peak shifting when the frequency varies). The $x = 2$ sample seems to be an exception but it has been confirmed that the apparent frequency dependence of the internal friction and modulus is caused by hydrogen interaction with martensite (R) twin boundaries [28,29].

At high Fe doping levels ($x = 6$, 6.5 and 7; i.e. the abnormal non-transforming compositions), the DMA results show a different behavior from that of the transforming compositions. Fig. 4d and e shows the DMA results of $x = 6$ and 6.5, respectively, with the corresponding DSC curve shown at the bottom of each figure. The storage modulus and internal friction of these two abnormal non-transforming compositions show clear frequency dependence at the DSC hump temperature. At higher doping level of $x = 7$ (Fig. 4f), the frequency-dependent feature of the internal friction peak remains the same but the peak itself becomes too low to be accurately measured. The storage modulus shows frequency dependence but without showing a dip.

The peak temperature T_g of the internal friction in $x = 6$ and 6.5 exhibits a frequency dependence following the Vogel–Fulcher relation:

$$\omega = \omega_0 \cdot \exp[-E_a/K_B(T_g - T_0)]$$

where T_0 is the ideal glass transition temperature, as shown in Fig. 4g and h). Such a behavior is characteristic of a strain glass transition [1,3] and cannot be explained by other types of transitions such as second order transitions or incommensurate–commensurate transitions. Therefore, doping Fe exceeding a critical concentration results in a crossover from a martensitic transformation into a strain glass transition. Such a result is similar to the case of $Ti_{50-x}Ni_{50+x}$ [1] binary and $Ti_{50}Pd_{50-x}Cr_x$ [9] ternary systems.

To further confirm that the system undergoes a strain glass transition when $x \geqslant 6$, a zero-field-cooling/field cooling (ZFC/FC) experiment was carried out for the alloy with $x = 6.5$. The results are shown in Fig. 5. With the decrease in temperature, the gap between the ZFC and FC curves increases gradually, indicating a continuous breaking of the ergodicity of the system – another important property of a glass transition [2,26]. The ZFC peak position in Fig. 5 corresponds to the peak freezing temperature T_f. It is noted that similar ZFC/FC curves have been found not only in Ti–Ni binary strain glass [2], but also in

Author's personal copy

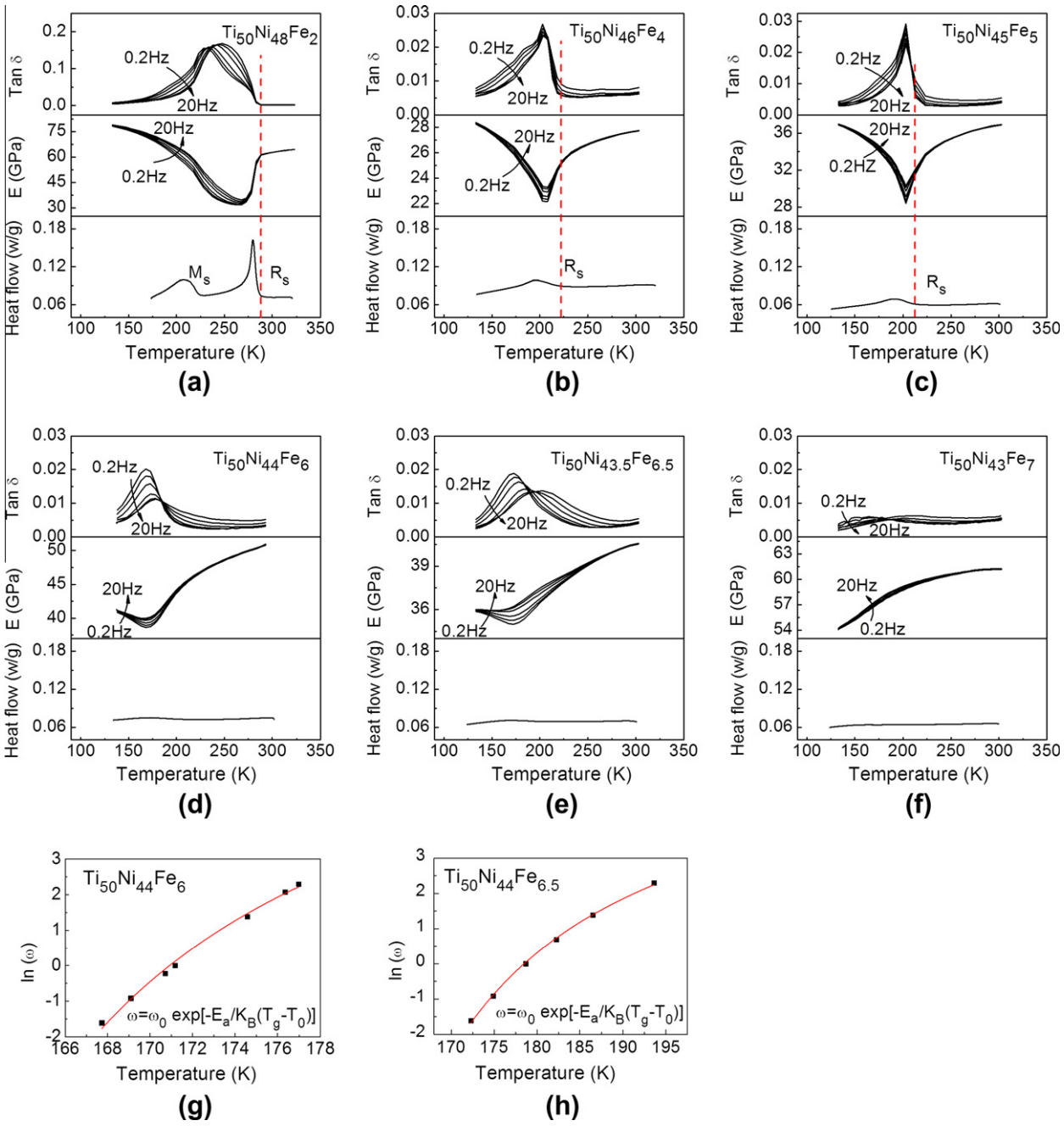

Fig. 4. DMA measurement of storage modulus (E) and internal friction (tan δ) of $Ti_{50}Ni_{50-x}Fe_x$ alloys at different x. The frequency is varied from 0.2 Hz to 20 Hz. For a comparison, the DSC results are also shown in the figures. (a) $Ti_{50}Ni_{48}Fe_2$, (b) $Ti_{50}Ni_{46}Fe_4$, (c) $Ti_{50}Ni_{45}Fe_5$, (d) $Ti_{50}Ni_{44}Fe_6$, (e) $Ti_{50}Ni_{43.5}Fe_{6.5}$ and (f) $Ti_{50}Ni_{43}Fe_7$. (g) and (h) describe the Vogel–Fulcher fitting for alloy $Ti_{50}Ni_{44}Fe_6$ and $Ti_{50}Ni_{43.5}Fe_{6.5}$, respectively.

various other kinds of ferroic glasses like relaxor [30] and cluster spin glass [31].

The above experiments have shown clearly that the abnormal non-transforming compositions (i.e. $x \geqslant 6$) actually correspond to strain glasses. Different from the Ni-rich Ti–Ni strain glasses where the nano-domains have an R-like structure [1] that is different from the corresponding martensite (B19′), the $Ti_{50}Ni_{50-x}Fe_x$ ($x \geqslant 6$) strain glasses have the same structure (R) as the corresponding martensite (R), as shown by the TEM diffraction patterns and diffuse scattering presented in Fig. 6. For the martensitic alloy with $x = 4$, Fig. 6a–c shows that the alloy transformed from B2 (without diffuse 1/3 spots) (Fig. 6a) to an R-martensite characterized by sharp and commensurate 1/3 spots (Fig. 6c) (typical for R-martensite), via a pre-martensitic state characterized by the appearance of diffuse incommensurate 1/3 spots (Fig. 6b). On the other hand, for the strain glass composition $x = 6$, the diffraction pattern reveals interesting but subtle changes, as shown in Fig. 6d. At room temperature ($T \gg T_0$), the alloy has a

Author's personal copy

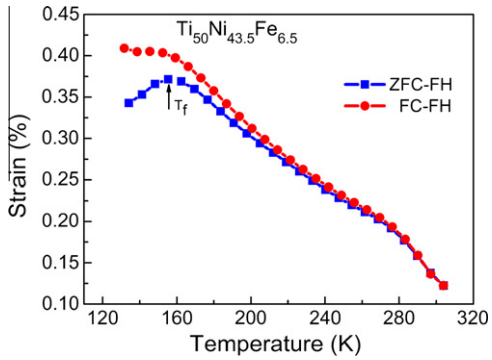

Fig. 5. ZFC/FC curves obtained for alloy $Ti_{50}Ni_{43.5}Fe_{6.5}$. The applied stress is about 30 MPa. The ZFC–FH peak position (indicated by the arrow) corresponds to the freezing temperature T_f.

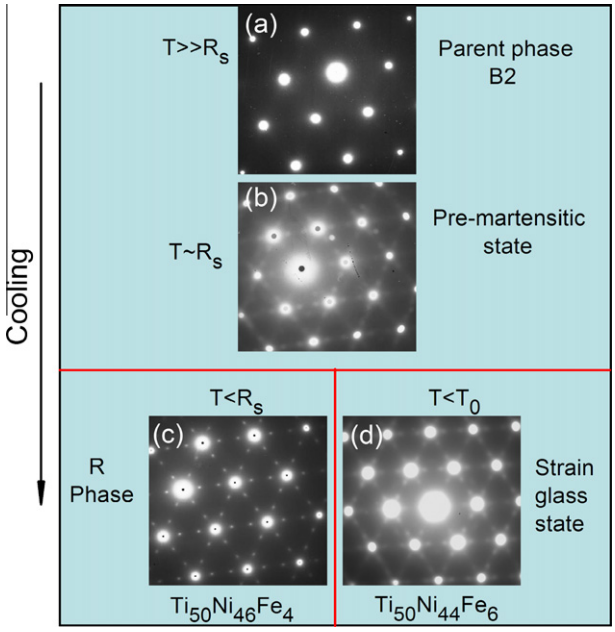

Fig. 6. TEM diffraction patterns of $Ti_{50}Ni_{46}Fe_4$ and $Ti_{50}Ni_{44}Fe_6$ alloys at different temperatures. (a)–(c) are, respectively, diffraction patterns of $Ti_{50}Ni_{46}Fe_4$ obtained at room temperature ($T \gg R_s$), $T \sim R_s$, and $T < R_s$. (d) is the diffraction pattern of $Ti_{50}Ni_{44}Fe_6$ below the strain glass transition temperature T_0.

B2 structure with no diffuse superlattice spots in the diffraction pattern (same as that shown in Fig. 6a). When the temperature is lowered, incommensurate 1/3 spots gradually appear and increase in their intensity [1,15]. These incommensurate 1/3 spots persist even down to $T \ll T_0$ (Fig. 6d). From the similarity of the incommensurate 1/3 spots of the pre-martensitic state and the strain glass state to the 1/3 spots of the normal R-martensite, it can be assumed that the structure in the nano-domains of the pre-martensitic and strain glass states is the same as or similar to the structure of the R-martensite.

The incommensuration in the pre-martenstic state and the strain glass state is likely to be caused by the small size of R domains mixed with the remaining B2 matrix. Under such a situation, the electron diffraction could show an averaging effect, making the positions of the superlattice spots no longer commensurate. Clearly, this interpretation of the incommensuration in the pre-martensitic state and in the strain glass state differs from previous hypothesis of an "incommensurate-to-commensurate transition" or a certain second order transition [15]. These hypotheses are inconsistent with the glass transition features shown in the DMA and ZFC/FC experiments.

Fig. 7 shows the cooling and heating curves obtained in the DSC, electrical resistivity [14,15] and DMA measurements carried out around the glass transition temperature for the alloy with $x = 6.5$. From the results one can see that there is no hysteresis associated with the strain glass transition, which is different from the martensitic transformation in $Ti_{50}Ni_{50-x}Fe_x$ system that shows a clear hysteresis. It is noted that there is a difference between the dip temperature in the resistivity vs. temperature curve (Fig. 7c) and that in the storage modulus vs. temperature curve (Fig. 7d). Electrical resistivity dip describes the temperature at which the resistivity caused by the increase of R nano-domain volume fraction compensates the decrease of resistivity caused by temperature decrease. On the other hand, storage modulus dip describes the temperature at which the system is essentially frozen. Clearly these two dips have very different physical origins, which therefore naturally do not coincide.

4. Discussion

4.1. Relations among various experimental signatures of a strain glass transition

The key result of the present work is the finding of a strain glass transition above a critical Fe doping level ($x \geqslant 6$). A strain glass transition shows two seemingly different facets if seen from different kinds of experimental measurements. On the one hand, the system appears non-transforming if seen from the invariance of the average structure (see XRD result of Fig. 1), the negligible heat dissipation (see DSC result of Fig. 2), and the absence of transformation hysteresis (see resistivity measurement in Fig. 3) [14,15]. On the other hand, it shows pronounced glass transition signatures and can be easily identified by DMA and ZFC/FC experiments (Figs. 4 and 5). Then an interesting question arises: what are the relationships among these "transforming" and "non-transforming" signatures?

Fig. 8 compares the DMA, electrical resistivity and ZFC/FC results obtained for $Ti_{50}Ni_{43.5}Fe_{6.5}$ during its strain glass transition. Fitting the frequency-dependent peak temperatures by the empirical Vogel–Fulcher law yields an ideal freezing temperature (i.e. the freezing temperature at 0 Hz) $T_0 \sim 150$ K. It is found that T_0 corresponds well to the inflection point, T_I, of the resistivity vs. temperature (R–T) curve, which is about 154 K. This ideal freezing temperature T_0 is also consistent with the peak temperature T_f measured in the ZFC curve. Therefore, the freezing temperature is reflected in different kinds

Author's personal copy

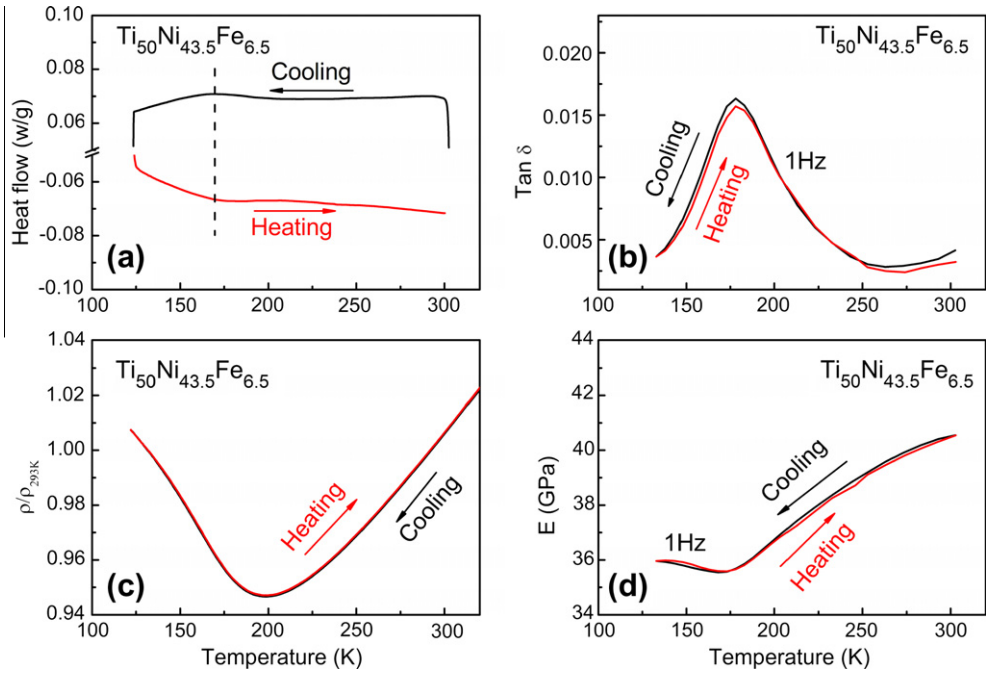

Fig. 7. Hysteresis properties of strain glass transition in $Ti_{50}Ni_{43.5}Fe_{6.5}$. (a) Heat flow curves; (b) electrical resistivity measurements; (c) internal friction with frequency 1 Hz; and (d) storage modulus with frequency 1 Hz.

of experimental measurements ($T_0 = T_I = T_f$). In the current paper, T_0 is used to represent the strain glass transition temperature.

Besides the ideal freezing temperature T_0, there exists another important temperature in a strain glass system, T_{nd} ("nd" stands for static "nano-domains"), at which the ergodicity starts to break. Note that T_{nd} is well above T_0. This temperature corresponds to the Burns temperature of relaxor ferroelectrics [32,33]. It is the temperature at which internal friction starts to increase (Fig. 8a) and the temperature at which the ZFC and FC curves start to deviate from each other (Fig. 8c). It is found that this ergodicity-breaking start temperature T_{nd} coincides with the temperature T_{IN} at which the electrical resistivity starts to deviate from linearity (Fig. 8b).

The microscopic process of a strain glass transition during cooling from $T > T_{nd}$ to $T_0 < T < T_{nd}$ to $T < T_0$ are illustrated in Fig. 8d. At high temperatures $T > T_{nd}$, there exist no static ferroelastic nano-domains despite the existence of randomly distributed local strains caused by point defects (indicated by the arrows). When the temperature is lowered to $T < T_{nd}$, some static nano-ferroelastic domains (local strain induced nano-domains) appear and the system starts to lose ergodicity. When the temperature is further decreased to $T < T_0$, the nano-domains are fully developed and are completely frozen. Then the ergodicity of the system is completely broken and the system becomes a strain glass.

The microscopic picture of the strain glass described above explains why a strain glass appears as "non-transforming" if measured with XRD and DSC. As the strain glass transition involves the formation and freezing of nano-sized ferroelastic domains, such a process does not cause a XRD peak splitting. This is why XRD does not show any obvious signature of a phase transition (Fig. 1c). Nevertheless, the growth of nano-domains causes a broadening of the XRD peak, as shown in Fig. 1d. On the other hand, the gradual evolution of the nano-domains extends over a wide temperature range (>100 K) and there is no abrupt change in entropy at any temperature; this leads to a negligible thermal effect in the DSC curve (Fig. 2).

Fig. 8 shows that the resistivity measurement, which is a simple technique, can be utilized to determine the important glass transition temperatures T_{nd} (T_{IN}) and T_0 (T_I). We shall later use this simple method to determine the phase diagram of the $Ti_{50}Ni_{50-x}Fe_x$ system.

4.2. Phase diagram of $Ti_{50}Ni_{50-x}Fe_x$ ferroelastic system

With the systematic measurements shown from Figs. 1 to 8, we are able to provide a new phase diagram for the $Ti_{50}Ni_{50-x}Fe_x$ ferroelastic system, as shown in Fig. 9. Compared with an early version of the phase diagram [27], the new phase diagram shows the following important features that have not been shown before:

(1) There exists a hitherto unknown state, strain glass, when $x \geqslant 6$.
(2) There exists a crossover from martensitic (including R) transformation to strain glass transition when Fe doping level exceeds 5 ($x \geqslant 6$). A more detailed measurement has found that the crossover occurs at $x \sim 5.5$ [34].

Author's personal copy

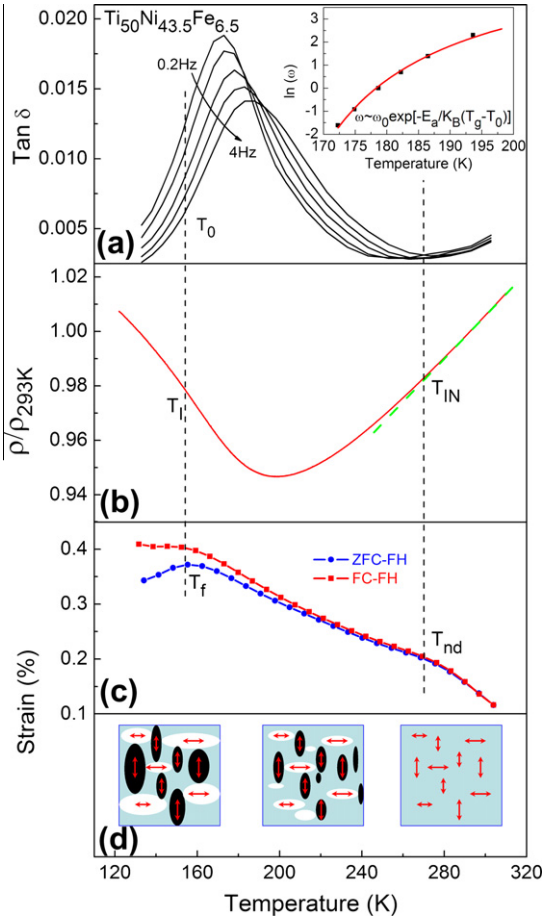

Fig. 8. Correlation among different characteristics of a strain glass transition. (a) Internal friction results with frequency 0.2–4 Hz; (b) electrical resistivity measurements; (c) ZFC/FC curves. The correspondence of inflection point position T_I in the electrical resistivity curve, the ideal strain glass transition temperature T_0 determined from the DMA measurements and the frozen temperature T_f identified by the ZFC/FC curves is indicated by the dashed line on the left. T_0 was obtained through fitting the experimental data to the Vogel–Fulcher law (see the inset in (a)). Another dashed line indicates the correspondence of the inflection point at high temperature ($T_{IN} \sim 270$ K) of the resistivity curve and the ergodicity-breaking start temperature T_{nd} shown in the ZFC/FC curves. (d) Schematic microscopic illustration of strain glass freezing process. The arrows represent the local strain states caused by point defect. The white and black colors represent different martensitic variants.

(3) In Fe-doped Ti–Ni alloys, quasi-static nano-domains start to appear at a temperature (T_{nd}) well above R_s (for $x < 5$) or T_0 (for $x \geqslant 6$). T_{nd} corresponds to the start of ergodicity-breaking and to the commonly known "pre-martensitic state" or "precursory nano-domains state".

In the strain glasses ($x \geqslant 6$), the freezing process of R-like nano-domains occurs between T_{nd} and T_0. The randomly distributed point defects play two important roles in the transition process: (a) they lower the thermodynamic stability of both nano-domains and long-range ordered structures (martensite) of the R-phase, which can be seen from the dependence of the phase transition temperatures

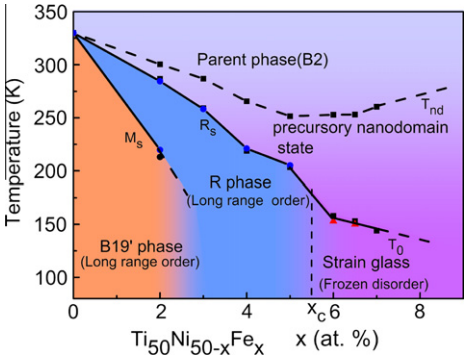

Fig. 9. Phase diagram of $Ti_{50}Ni_{50-x}Fe_x$ ferroelastic system (color online). The blue circles show the phase transformation temperatures from DSC results, the red triangles describe the glass transition temperature T_0 obtained through fitting the DMA results and the black squares are the phase transformation temperatures determined from the electrical resistivity curves. R_s and M_s are the normal R-phase and B19′ phase martensitic transformation temperatures, T_{nd} is the start of ergodicity-breaking temperature, and T_0 is the strain glass transition temperature. (For interpretation of the references to colour in this figure legend, the reader is referred to the web version of this article.)

on defect concentration (R_s or M_s vs. x); (b) they promote the freezing of the R-phase nano-domains once they form (i.e. convert dynamic domains into static ones), which can be seen from the T_{nd} vs. x curve on the phase diagram. It should be noted that T_{nd} is the temperature at which quasi-static R-like nano-domains start to appear (or the onset of ergodicity-breaking), which is different from M_s (or R_s). The latter represents thermodynamic stability of martensite (long-range order). Increasing point defect concentration x lowers the thermodynamic stability of martensite and hence lowers M_s (or R_s). However, the onset of quasi-static nano-domains is dependent on both thermodynamic stability of martensite (R) and the local stress/strain field caused by point defects (i.e. the local field effect). At high defect concentrations, the local field effect becomes dominant and T_{nd} increases with defect concentration.

It should be noted that the nano-domains of the strain glass have an R-like structure, which is the same as the corresponding R-martensite in the neighboring regime of the phase diagram. Therefore, the short-range strain order of this system is the same as the long-range strain order (R-martensite). This situation is different from the case of Ni-rich Ti–Ni, where the system has an R-like short-range strain order but a B19′ martensite. Similar situation has been found in relaxor ferroelectrics [35,36], where the long-range order can be either the same as or different from the short-range order. Whether the short-range strain order in strain glass is the same as the long-range strain order in martensite depends on how the point defects alter the transformation path. It is obvious that Fe-doped Ti–Ni system prefers both short-range and long-range order R, while excess N-doped Ti–Ni system prefers short-range order R and long-range order B19′. The same short-range and long-range strain order makes $Ti_{50}Ni_{50-x}Fe_x$ system

Author's personal copy

an ideal or prototypical system for establishing strain glass theories.

With this new phase diagram, all the previous puzzles about the Ti–Ni–Fe system, such as the abnormal non-transforming compositions, the negative temperature dependence of electrical resistivity, and the nature of the pre-martensitic nano-domains, can be easily understood.

4.3. Origin of negative temperature dependence of electrical resistivity

A negative temperature dependence (NTD) of electrical resistivity is characteristic of insulators rather than metals. However, Ti–Ni–Fe and Ni-rich Ti–Ni systems exhibit NTD in martensitic alloys prior to the martensitic transformation and in the abnormal non-transforming alloys [13–15,21,22] (now proven to be strain glasses). Such abnormal behavior has been studied through the first principle simulation in the frame of electronic structure recently [21,22]. Now with the relationship between the resistivity and the microscopic picture of the strain glass established in this study (Fig. 8d), we could offer a simple phenomenological explanation for the NTD of the alloys with $x \geqslant 6$.

The understanding of NTD can be derived from the following three important facts: (1) ferroelastic nano-domains start to appear at T_{nd} and gradually increase in size and volume fraction with decreasing temperature, as shown in Fig. 8d; (2) the nano-domains have R-phase structure, as suggested by the 1/3 superlattice diffraction spots (Fig. 6); (3) the R structure has a higher specific electrical resistivity than that of the B2 parent phase, as can be seen from Fig. 3. At $T > T_{nd}$, the system exhibits a normal metallic behavior, i.e. having a positive temperature dependence of resistivity. Below T_{nd}, nano-sized R-domains with higher specific resistivity start to form and increase gradually in volume fraction. This leads to an opposite effect from the normal phonon scattering effect in metals, as shown in Fig. 8b. With further decrease in temperature, the volume fraction of the R-like nano-domains further increases and their positive contribution to the resistivity eventually exceeds the phonon scattering effect. As a result, the resistivity increases with decreasing temperature when the temperature is well below T_{nd}, as shown in Fig. 8b.

A similar NTD phenomenon has been reported for Ni-rich Ti–Ni and Ti–Ni–Fe martensitic systems prior to their martensitic transformation temperatures [13–15] (also observed in the current study for $Ti_{50}Ni_{46}Fe_4$). The physical origin is the same as the one discussed above for strain glasses. For example, nano-sized R domains appear well above the martensitic transformation temperature in these systems (e.g. $T_{nd} \gg M_s$ (or R_s)) [16] and the NTD is caused by gradual increase in volume fraction of the R-like nano-domains prior to the martensitic transformation.

It should be noted that different views on the nature of these effects exist [21,22], which consider that such resistivity anomaly is caused by nesting effect of Fermi surface. But our strain glass scenario seems to provide a consistent explanation for all the properties observed, including thermal, mechanical, and electrical properties.

5. Summary

Strain glass transitions were discovered in Fe-doped ternary $Ti_{50}Ni_{50-x}Fe_x$ alloys when x exceeds a critical value x_c ($5 < x_c < 6$). With the discovery of strain glass transition in this well-studied system, all previous puzzles associated with these abnormal non-transforming alloys ($x > x_c$) can now be explained, such as the broad hump in DSC curves, abnormal negative temperature dependence (NTD) of electrical resistivity. A complete temperature–composition phase diagram was established, which includes pre-martensitic state, martensite and strain glass.

Acknowledgements

The authors gratefully acknowledge the support of National Natural Science Foundation of China (50720145101, 50771079), National Basic Research Program of China (2010CB613003), and 111 Project of China, China Scholarship Council and the US National Aeronautics and Space Administration (NASA) under grant NNX08AB49A and the National Science Foundation under MWN program (DMR 1008349) (Y. Wang). The authors are grateful to Y.C. Ji for the contribution to Fig. 4a.

References

[1] Sarkar S, Ren X, Otsuka K. Phys Rev Lett 2005;95:20572.
[2] Wang Y, Ren X, Otsuka K, Saxena A. Phys Rev B 2007;76:132201.
[3] Mydosh JA. Spin glasses. London: Taylor & Francis; 1993.
[4] Binder K, Young AP. Rev Mod Phys 1986;58:801.
[5] Cross LE. Ferroelectrics 1987;76:241.
[6] Vugmeister BE, Rabitz H. Phys Rev B 1998;57:7581.
[7] Samara GA. J Phys Condens Matter 2003;15:R367.
[8] Wang Y, Ren X, Otsuka K. Phys Rev Lett 2006;97:225703.
[9] Zhou Y, Xue D, Ding X, Otsuka K, Sun J, Ren X. Appl Phys Lett 2009;95:151906.
[10] Murakami Y, Shindo D. Philos Mag Lett 2001;81:631.
[11] Shapiro SM, Larese JZ, Noda Y, Moss SC, Tanner LE. Phys Rev Lett 1986;57:3199.
[12] Semenovskaya S, Khachaturyan AG. Acta Mater 1997;45:4367.
[13] Kakeshita T, Fukuda T, Tetsukawa H, Saburi T, Kindo K, Takeuchi T, et al. Jpn J Appl Phys 1998;37:2535.
[14] Choi MS, Fukuda T, Kakeshita T. Scripta Mater 2005;53:869.
[15] Choi MS, Fukuda T, Kakeshita T, Mori H. Philos Mag 2006;86:67.
[16] Kartha S, Castán T, Krumhansl JA, Sethna JP. Phys Rev Lett 1991;67:3630.
[17] Kartha S, Krumhansl JA, Sethna JP, Wickham LK. Phys Rev B 1995;52:803.
[18] Ren X, Wang Y, Zhou Y, Zhang Z, Wang D, Fan G, et al. Philos Mag 2010;90:141.
[19] Shindo D, Murakami Y, Ohba T. MRS Bull 2002;27:121.
[20] Murakami Y, Shibuya H, Shindo D. J Microsc 2001;203:22.
[21] Manley ME, Asta M, Lashley JC, Retford CM, et al. Phys Rev B 2008;77:024201.
[22] Yamamoto T, Choi MS, Majima S, Fukuda T, et al. Philos Mag 2008;88:1027.
[23] Ren X, Wang Y, Otsuka K, Lloveras P, Castán T, Porta M, et al. MRS Bull 2009;34:838.

Author's personal copy

[24] Otsuka K, Ren X. Prog Mater Sci 2005;50:511.
[25] Otsuka K, Wayman CM. Shape memory materials. Cambridge: Cambridge University Press; 1998.
[26] Wang Y, Ren X, Otsuka K, Saxena A. Acta Mater 2008;56:2885.
[27] Honma T, Matsumoto M, Shugo Y, Nishida M, Yamazaki I. In: Kimura H, Izumi O, editors. Proc 4th int conf on titanium, Kyoto. AIME; 1980. p. 1455.
[28] Fan G, Zhou Y, Otsuka K, Ren X. Appl Phys Lett 2006;89:161902.
[29] Fan G, Zhou Y, Otsuka K, Ren X, Nakamura K, Ohba T, et al. Acta Mater 2006;54:5221.
[30] Viehland D, Li JF, Jang SJ, Cross LE, Wuttig M. Phys Rev B 1992;46:8013.
[31] Gayathri N, Raychaudhuri AK, Tiwary SK, Gundakaram R, Arulraj A, Rao CNR. Phys Rev B 1997;56:1345.
[32] Burns G, Dacol FH. Solid State Commun 1983;48:853.
[33] Burns G, Scott VA. Solid State Commun 1973;13:423.
[34] Zhang J, Ren X, et al. submitted for publication.
[35] Dkhil B, Kiat J, Calvarin G, Baldinozzi G, Vakhrushev S, Suard E. Phys Rev B 2001;65:024104.
[36] Marssi M, Farhi R, Viehland D. J Appl Phys 1997;81:355.